

Dynamics at the quasiperiodic onset of chaos, Tsalis q -statistics and Mori's q -phase thermodynamics

H. Hernandez-Saldana and A. Robledo^y

Instituto de Física,

Universidad Nacional Autónoma de México,

Apartado Postal 20-364, México 01000 D.F., México.

(Dated: .)

We analyze the dynamics along the golden-mean route to chaos in the critical circle map and find that trajectories within the attractor at the chaos threshold consist of infinite sets of power laws mixed together. We elucidate this structure assisted by known renormalization group (RG) results. We find that the sensitivity to initial conditions ϵ_t has the form of families of intertwined q -exponentials, of which we determine the q -indexes and the generalized Lyapunov coefficient spectra λ_q . Further, the dynamics within the critical attractor is found to consist of a collection of Mori's q -phase transitions with a hierarchical structure. The value of q at each transition corresponds to the same special value for the entropic index q .

PACS numbers: 05.45.Ac, 05.90.+m, 05.10.Lc

I. INTRODUCTION

Critical attractors of nonlinear low-dimensional maps have always drawn much interest because they demonstrate the ways by which nonlinear systems bridge periodic and chaotic motion [1]–[3]. The geometrical properties of these attractors are well known since long ago [1]–[3], but their dynamical properties are even now perplexing and are still in need of full understanding. In addition, renewed interest in this subject [4]–[15] has focused on the applicability of q -statistics, the generalization of the Boltzmann-Gibbs (BG) statistical mechanics proposed by Tsalis [16], [17], to these nonlinear systems. Important examples of critical attractors are the onset of chaos via period doubling, intermittence and quasiperiodicity, the three universal routes to chaos in dissipative maps displayed by the prototypical logistic and circle maps [1]–[3]. Perhaps the most interesting types of critical attractors are critical strange nonchaotic attractors [18] as in the period doubling and quasiperiodic onset of chaos. These are geometrically involved multifractal attractors with a vanishing Lyapunov coefficient λ_1 and a sensitivity to initial conditions ϵ_t that does not converge to any single-valued function but instead displays a fluctuating pattern that grows as a power law in time t [19]–[23].

Trajectories within a critical attractor show self-similar temporal structures, they preserve memory of their previous locations and do not have the mixing property of truly chaotic trajectories [23]. Recently, rigorous results have been developed [8]–[15] about the validity of q -statistics (outlined in the next paragraph) for the critical attractors associated to the intermittency and period-doubling routes to chaos, i.e. the tangent bifurcation and

the accumulation point of the pitchfork bifurcations, but studies of the same type have not been carried out for the quasiperiodic route to chaos. Here we present results on this route by considering the proverbial golden-mean onset of chaos in the critical circle map [1], [3] and show that there are elements of universality in their dynamical properties as they appear in close correspondence with those recently analyzed for the Feigenbaum attractor [15].

The central point of the q -statistics with regards to the description of the dynamics of critical attractors is a sensitivity to initial conditions ϵ_t associated to the q -exponential functional form, i.e. the ' q -deformed' exponential function $\exp_q(x) = [(q-1)x]^{1/(q-1)}$ [4], [5]. From such ϵ_t one or several spectra of q -generalized Lyapunov coefficients λ_q can be determined [9], [15]. The λ_q are dependent on the initial position and each spectrum can be examined by varying this position. The λ_q satisfy an identity $\lambda_q = K_q$ where K_q is an entropy production rate based on the Tsalis entropy S_q , defined in terms of the q -logarithmic function $\ln_q y = (\ln y)^{1/(q-1)} = (1-q)$, the inverse of $\exp_q(x)$ [4], [9], [15].

We find that ϵ_t at the golden-mean onset of chaos takes the form of a family of interwoven q -exponentials. The q -indexes appear in conjugate pairs, q and $Q = 2 - q$, as these correspond to switching starting and finishing trajectory positions. We show that q and Q are related to the occurrence of pairs of dynamical ' q -phase' transitions that connect qualitatively different regions of the attractor [21]–[23]. These transitions are identified as the source of the special values for the entropic index q . The allowed values of the entropic index q are obtained from the universality class parameters to which the attractor belongs, in our present case these are the golden-mean winding number $w_{gm} = (\sqrt{5} - 1)/2 = 0.618034$ and the universal constants (in the sense of Feigenbaum's trajectory scaling function [24]–[26]) that measure the power-law clustering of iterate positions, the most prominent of which is $\delta_{gm} = 1.288575$, that is associated to

^Electronic address: hugo@fisica.unam.mx

^yElectronic address: robledo@fisica.unam.mx

the most rare and (as $\frac{3}{g_m}$) the most crowded regions of the multifractal attractor.

We are interested here in determining the detailed dependence of the aforementioned dynamical structure for the golden-mean chaos threshold on both the initial position and the observation time as this dependence is preserved by the infinite memory of trajectories. To this purpose we recall in the following Section 2 the familiar features of the circle map, and the properties of the renormalization group (RG) fixed-point map for a cubic inflection point with zero slope. Then in Section 3 we describe the organization of the superstable trajectory at the chaos threshold into families of positions that fall onto power laws in time. Assisted by these properties, in Section 4 we determine the sensitivity ϵ_t for trajectories within the multifractal attractor that connect its most crowded and sparse regions. In Section 5 we explain how the properties for ϵ_t and its q -spectrum are related to the occurrence of dynamical q -phase transitions and corroborate previously obtained numerical results. In Section 6 we express ϵ_t in terms of the discontinuities of the trajectory scaling function that measures local contraction rates within the multifractal attractor. From this relationship we obtain results for trajectories that involve other multifractal regions and show that the dynamics consists of a hierarchy of q -indexes and q -phase transitions. In Section 7 we summarize our results.

II. THE GOLDEN-MEAN ONSET OF CHAOS

To assist our presentation in the following sections we recall here basic features of the circle map [1], [3]. The map is given by

$$f_{;K}(\theta) = \theta + K \sin 2\pi\theta \pmod{1}; \quad (1)$$

where the control parameters θ and K are the bare winding number and the amount of nonlinearity, respectively. An important parameter for the description of the structure of the trajectories of this map is the dressed winding number

$$w = \lim_{t \rightarrow \infty} \frac{f^t(\theta) - \theta}{t}; \quad (2)$$

the average increment of $f^t(\theta)$ per iteration. The map is monotonic and invertible for $K < 1$, develops a cubic inflection point at $\theta = 0$ (or $\theta = 1$, see Figs. 1) for $K = 1$, and becomes nonmonotonic and noninvertible for $K > 1$. For $K < 1$ trajectories are periodic (locked motion) when w is rational and quasiperiodic (unlocked motion) when w is irrational. The winding number $w(\theta)$ forms a 'devil's staircase' making a step at each rational $p=q$ and remaining constant $w = p/q$ for a range of θ . For $K = 1$, the critical circle map, locked motion covers the entire θ interval leaving only a multifractal set of unlocked θ ; the quasiperiodic solutions become the chaos threshold. For $K > 1$ the regions of periodic motion (Arnold tongues) overlap leading to chaotic motion.

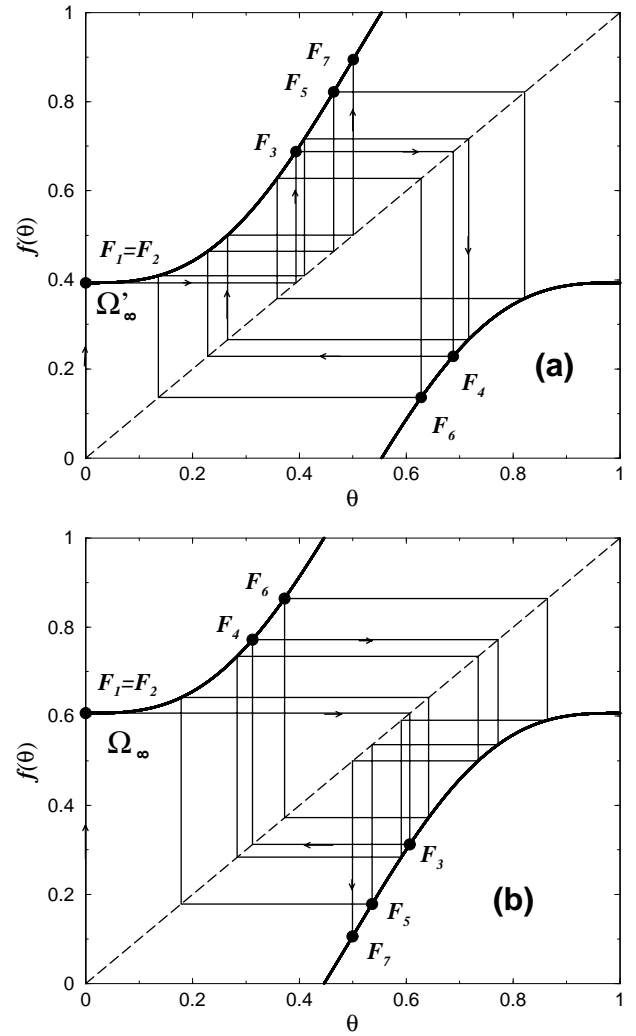


FIG. 1: Critical circle map $K = 1$ and supercycle trajectories. a) $w = \frac{1}{5}$. b) $w = \frac{1}{2}$. The labels F_n correspond to trajectory times given by Fibonacci numbers.

A standard way to study the quasiperiodic route to chaos is to fix the value of $K = 1$ and select an irrational w . Then a choice is made of successive rational values for w to obtain an infinite sequence of winding numbers that approach w . A convenient sequence of such rational values for w are given by consecutive truncations of the continued fraction expansion of w . A well-studied, and perhaps the most interesting, case is the sequence of rational approximants to $w_{gm} = (\sqrt{5} - 1)/2 = 0.618034$, the reciprocal of the golden mean, that yields the winding numbers $w_n = F_{n+1}/F_n$, where F_n are the Fibonacci numbers $F_{n+1} = F_n + F_{n-1}$. Within the range of w for which $w = F_{n+1}/F_n$ one observes trajectories of period F_n , and therefore a route to chaos consists of an infinite family of periodic orbits with increasing periods of values F_n , $n \geq 1$. It has proved useful to single out from these families the periodic trajectories with the 'superstable' property, i.e. orbits that contain the po-

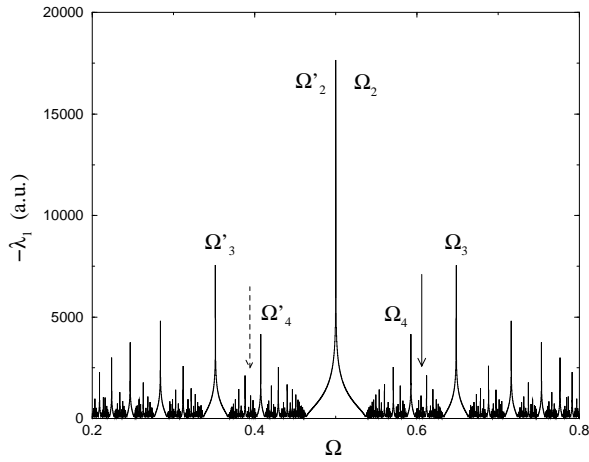


FIG. 2: The Lyapunov coefficient $-\lambda_1$ for the critical circle map $K = 1$ as a function of winding number. The supercycle divergences to 1 can be clearly appreciated and the locations for the two accumulation points at Ω'_1 and Ω_1 are indicated by the arrows.

sition $\omega = 0$ and have a Lyapunov coefficient $-\lambda_1$ that diverges to 1 . Thus, the superstable orbits appear for values ω_n , $n = 1; 2; \dots$, at which the derivative of $f_{n;1}(\omega)$ at $\omega = 0$ vanishes. The ω_n are obtained from $f_{n;1}^{F_n+1}(0) = F_n$, and lie on zigzag paths approaching the limit $\omega_1 = 0.606661$ which corresponds to w_{gm} . As the golden mean w_{gm} arises from the condition $w = 1 - w^2$, a second superstable family of trajectories is determined by considering the winding numbers $w_n^0 = F_{n-2} = F_n$, with ω_n^0 , $n = 1; 2; \dots$, obtained in turn from $f_{n;1}^{F_n+1}(0) = F_{n-1}$. The ω_n^0 converge to $\omega_1^0 = 1 - \omega_1 = 0.393339$ which corresponds to $w_{gm}^2 = 0.381966$. In Figs. 1a and 1b we show the critical map for $\omega = \omega_1^0$ and $\omega = \omega_1$, respectively, together with a portion of the superstable trajectory at the chaos threshold. In Fig. 2 we show the values for the Lyapunov coefficients $-\lambda_1$ for $K = 1$ as a function of ω where the locations of the two superstable families are clearly seen and those for their accumulation points are indicated.

A celebrated development [1], [3] dating from the early 80's is the recognition that the quasiperiodic route to chaos displays universal scaling properties. The analysis was based on an RG approach analogous to that for the period doubling cascade, and can be suitably discussed in terms of the critical circle map. The universal properties are obtained from the fixed-point map $g(\omega)$ of an RG transformation that consists of functional composition and rescaling appropriate for maps with a zero-slope cubic in action point. The fixed-point map satisfies

$$g(\omega) = w_{gm} g(w_{gm} g(\omega - w_{gm}^2)); \quad (3)$$

where $w_{gm} = 1.288575$ is a universal constant [1], [3]. This constant describes the scaling of the distance d_n from $\omega = 0$ to the nearest element of the orbit with w_n , i.e. $d_n = f_{n;1}^{F_n}(0) - F_{n-1}$. The scaling is given

by $\lim_{n \rightarrow \infty} (d_n - d_{n+1}) = w_{gm}$. Associated to the chaos threshold at the golden mean w_{gm} there is a multifractal set (the attractor) that measures the different degrees of clustering of iterate positions. This multifractal has a dimension spectrum $f(\alpha)$ within a range of values between α_{min} and α_{max} [27]. The most rarefied region of the multifractal corresponds to $\alpha_{max} = \ln w_{gm} = \ln j_{gm} = 1.897995$, and this region is mapped onto the multifractal's most crowded region characterized by $\alpha_{min} = -\ln w_{gm} = 3 \ln j_{gm} = 0.632665$ [27]. The chaos threshold for special values of the winding number is known as local universality [1].

III. STRUCTURE OF TRAJECTORIES WITHIN THE ATTRACTOR

We consider the last of the superstable trajectories, with infinite period when $\omega = \omega_1$ or ω_1^0 and starting at $(0) = 0$. As we shall see all other trajectories within the attractor can be obtained from it. We find convenient to plot the positions $\omega(t)$ and their iteration time t in logarithmic scales as shown in Figs. 3a and 3b, obtained for ω_1 and ω_1^0 , respectively, and where the labels record the times at which positions are reached. A distinctive feature in these figures is that positions fall along straight diagonal lines, an indication of embedded power law behavior. Notice that the positions of the main diagonal in Fig. 3a correspond to the times F_{2n} , $n = 1; 2; 3; \dots$. The succeeding diagonals above it appear grouped together. Above the main diagonal there are $k = 2$ close-by diagonals the first with positions that correspond to times of the form $2F_{2n}$ and the second for times of the form $F_{2n} + F_{2n-2}$. Above these two diagonals there is a group of $k = 3$ diagonals and above them a group of $k = 4$, etc. The times for the positions along each diagonal in the group of k diagonals are, from the bottom to the top, of the form kF_{2n} , $(k-1)F_{2n} + F_{2n-2}$, $(k-2)F_{2n} + 2F_{2n-2}, \dots, F_{2n} + (k-1)F_{2n-2}$, $n = 1; 2; 3; \dots$. The same structure is observed in Fig. 3b with F_{2n} replaced by F_{2n+1} . The slope shared by all the diagonal straight lines in Figs. 3a and 3b is $-\ln j_{gm} = -\ln w_{gm}$. Note too that the positions for F_{2n} in Fig. 3a appear along the top of Fig. 3b and approach asymptotically the horizontal line $\omega = 1$. And viceversa, the positions for F_{2n+1} in Fig. 3b appear along the top of Fig. 3a and approach asymptotically the horizontal line $\omega = 1$. Analogous features hold for the positions of the groups of subsequences with $k > 1$. A similar pattern of time subsequence positions arranged along parallel decreasing straight lines is observed in the plot of $\ln j_1(\omega(t))$ vs $\ln t$ (or identically, $\ln j_1^0(\omega(t))$ vs $\ln t$) that is shown in Fig. 4. As it can be observed there, the power-law diagonals along which positions fall appear again arranged in groups, each with an increasing number of members $k = 1; 2; 3; \dots$. The times for the positions along the group of k diagonals are, from the bottom to the top, of the form $kF_n + 1$, $(k-1)F_n + F_{n-2} + 1$, $(k-2)F_n + 2F_{n-2} + 1, \dots$

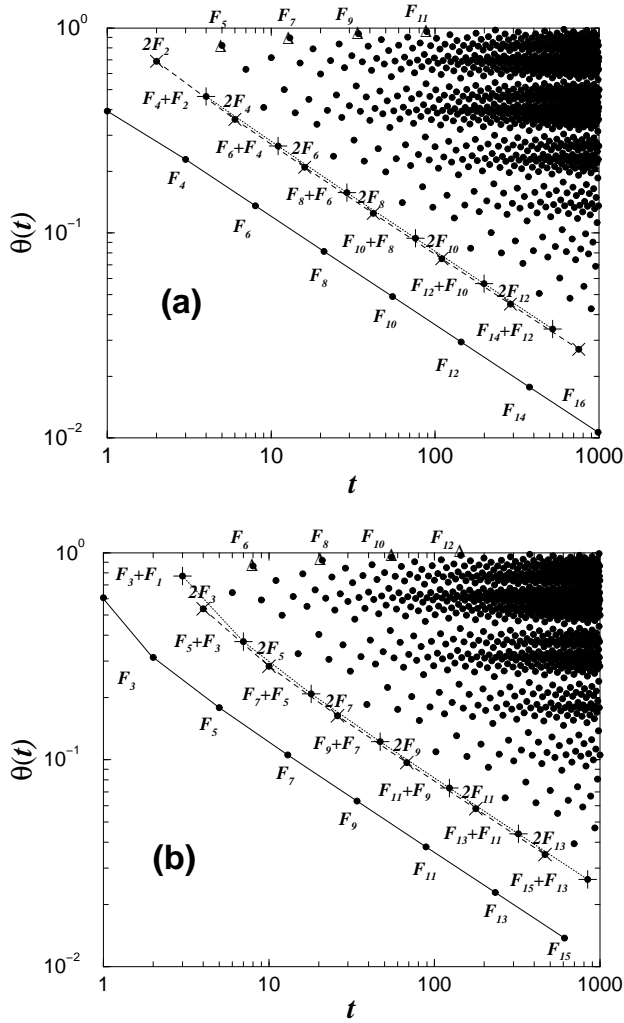


FIG. 3: a) Positions $\theta(t)$ vs t in logarithmic scales for the orbit with initial condition $\theta(0) = 0$ at θ_1^0 of the critical circle map $K = 1$. The lines are guides to the eye. The labels indicate iteration time t , the dashed line and symbols \circ correspond to times of the form $2F_{2n}$, and the dotted line and symbols $+$ correspond to times of the form $F_{2n} + F_{2n-2}$. The symbols \bullet correspond to the main diagonal positions at F_{2n+1} in (b). b) Same as a) with θ_1^0 replaced by θ_1^1 . The dashed line and symbols \circ correspond to times of the form $2F_{2n+1}$, and the dotted line and symbols $+$ correspond to times of the form $F_{2n+1} + F_{2n-1}$. The symbols \bullet correspond to the main diagonal positions at F_{2n} in (a). See text for description.

$F_n + (k-1)F_{n-2} + 1, n = 1; 2; 3; \dots$, and the slope shared by all the diagonals is $3 \ln j_{\text{gm}} - k \ln w_{\text{gm}}$.

More specifically, the trajectory starting at $\theta(0) = 0$ maps out the attractor in such a way that the values of succeeding (time-shifted $\theta = t+1$) positions form subsequences with a common power-law decay of the form $t^{-1/Q}$ with $Q = 1/\ln w_{\text{gm}} = \ln j_{\text{gm}} - k \ln w_{\text{gm}}$. (To avoid confusion we denote as $\theta(t)$ position at time t and as $\theta(t)$ the same position at shifted time t). That

is, the entire attractor can be decomposed into position subsequences generated by the time subsequences $\theta = (k-1)F_n + F_{n-2}$, each obtained by running over $n = 1; 2; 3; \dots$ for fixed values of $k = 1; 2; 3; \dots$ and $l = 0; 1; 2; \dots; k-1$. Noticeably, the positions for these subsequences can be asymptotically obtained from those belonging to the 'superstable' periodic orbits of lengths F_n at θ_n^0 or θ_n^1 . In particular, the positions for the main subsequence $k=1$, that constitutes the lower bound of the entire trajectory, can be identified to be F_n , $\theta_n^j = j_{\text{gm}} j^n$, $\theta_n^j = \theta_n^0$. The positions for each time subsequence that leads a group, $k-1$ and $l=0$, i.e. $\theta = kF_n$ in Figs. 3 and $\theta = kF_n + 1$ in Fig. 4, can be expressed, when use is made of the time shift $\theta = t+k$ and

$$\frac{F_n}{F_{n-1}} \frac{F_{n-1}}{F_{n-2}} \dots \frac{F_2}{F_1}, w_{\text{gm}}^n; \quad (4)$$

as

$$\theta = k \exp_{Q^+} \left(\frac{(k)}{Q^+} t \right); \quad (5)$$

with $\frac{(k)}{Q^+} = \ln j_{\text{gm}} - k \ln w_{\text{gm}}$, and

$$j_1 = j_1 - k j \exp_{Q^+} \left(\frac{(k)}{Q^+} t \right); \quad (6)$$

with $\frac{(k)}{Q} = 3 \ln j_{\text{gm}} - k \ln w_{\text{gm}}$, respectively. Interestingly, these analytical results can be seen to satisfy the dynamical scaling relation,

$$h = 1 - (1/Q) g(1 - (1/Q)); \quad (7)$$

with $h = \frac{1}{Q}$ or $j_1 = j$ where $\theta = k w_{\text{gm}}^n$ with $w_{\text{gm}} = \frac{1}{Q^+}$ or $w_{\text{gm}} = \frac{3}{Q}$, and where g is the fixed-point map with $\theta = k$ or $j_1 = k j$. The similarities with the dynamical properties of the supercycle orbit 2^1 at the Feigenbaum attractor are remarkable, see Refs. [8], [9] for the quadratic map and Refs. [10], [15] for its generalization to general nonlinearity $z > 1$.

IV. SENSITIVITY TO INITIAL CONDITIONS

We have now elements to derive the sensitivity to initial conditions $\theta(t)$, defined as $\theta(t) = \theta(0) + d(t) - d(0)$, when either $\theta(0) \neq 0$ or $\theta(0) = 1$. For simplicity of presentation we consider the case of the leading position subsequences within each group k , those for times $\theta = kF_n$ as described in the previous section. The results for the other subsequences within each group are similar and we only quote the differences in the expressions. We proceed in the following way. Recall [28] that

$$f_n(\theta) = \frac{n}{\text{gm}} g\left(\frac{n}{\text{gm}}\right); \quad \theta > 0; \quad (8)$$

where $f_n(\theta) = \frac{F_n}{n}; 1(\theta) = F_{n-1}$, and consider the lower-order terms in the expansion of $g\left(\frac{n}{\text{gm}}\right)$, i.e.

$$g\left(\frac{n}{\text{gm}}\right) = g(0) + \frac{1}{6} g'''(0) \frac{3n}{\text{gm}}^3; \quad (9)$$

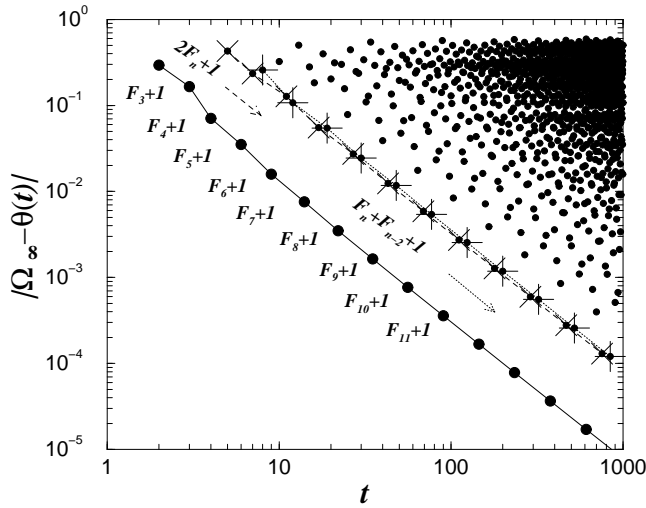


FIG. 4: Positions $j_k(t)$ vs t in logarithmic scales for the orbit with initial condition $(0) = 0$ at θ_1 of the critical circle map $K = 1$. The labels indicate iteration time t . The dashed line and symbols \circ correspond to times of the form $2F_n + 1$, and the dotted line and symbols $+$ correspond to times of the form $F_n + F_{n-2} + 1$. The same results are obtained with θ_1 replaced by θ_1^0 . See text for description.

If we denote the starting positions of two nearby trajectories at time $t = k$ by

$$k = f_1(\theta) + \frac{1}{6}g^{(k)}(0)^3 \quad (10)$$

and

$$k = f_1(\theta) + \frac{1}{6}g^{(k)}(0)^3; \quad (11)$$

their positions at time $t = kF_n$ are given by

$$kF_n = f_n(\theta) + \frac{1}{6}g^{(k)}(0)^{2n} \quad (12)$$

and

$$kF_n = f_n(\theta) + \frac{1}{6}g^{(k)}(0)^{2n}; \quad (13)$$

From the above we obtain

$$\frac{j_{kF_n}}{j_k} = \frac{j_{kF_n}}{j_k} = j_{gm}^{2n}; \quad (14)$$

For each subsequence k , the sensitivity t_k , given for the trajectories considered by

$$t_k = \lim_{j \rightarrow 0} \frac{j_{kF_n}}{j_k}; \quad (15)$$

can be written, with use of the shifted time variable t_k , and observing that

$$j_{gm}^{2n} = 1 + \frac{t_k}{k}; \quad (16)$$

as the q -exponential

$$t_k = \exp_q \left(\frac{t_k}{k} \right); \quad (17)$$

where

$$q = 1 + \frac{\ln w_{gm}}{2 \ln j_{gm}}; \quad 0.051003 \quad (18)$$

and

$$\frac{t_k}{k} = 2 \frac{\ln j_{gm}}{k \ln w_{gm}}; \quad (19)$$

The value of q in Eq. (18) agrees with that obtained in earlier studies [5]-[7].

The departing positions, $(0) = 0$ (or $(0) = 1$), for t_k in Eq. (17) are located in the most crowded region of the attractor and the value of k in $\frac{t_k}{k}$ in Eq. (17) locates this position as the top position with time label $t_k = kF_n$ of the subsequences described by the times $t_k = kF_n$ in Figs. 3a and 3b. By construction, the observation times in Eq. (17) are precisely $t_k = kF_n$ when the iterate is close to the most sparse region of the attractor, $(0) = 1$ (or $(0) = 0$). The sensitivity t_{k+1} for the inverse trajectories, with departing positions at the most sparse region and with observation times when at the most crowded region, can be evaluated in the same way as above, with the result

$$t_{k+1} = \exp_{2q} \left(\frac{t_{k+1}}{2k} \right); \quad (20)$$

with q as above and where

$$\frac{t_{k+1}}{2k} = \frac{2 \ln j_{gm}}{k w_{gm} \ln w_{gm}}; \quad (21)$$

Trajectories expand in one direction and contract in the opposite one. We recall that $\exp_q(x) = 1 + \exp_{2q}(x)$. The factor of w_{gm}^2 in $\frac{t_{k+1}}{2k}$ appears because of a basic difference between the orbits of periods F_n and F_1 . In the latter case, to reach $(0) = 0$ from $(0) = 1$ at times $t^0 = F_n + 1$ the iterate necessarily moves into positions of the next period F_{n+1} , and orbit contraction is w_{gm}^2 as effective than expansion. When considering the other sets of positions within each group of subsequences one obtains the same results as in Eqs. (17) to Eq. (21) with k replaced by $(k-1) + \ln w_{gm}^2$ in Eqs. (19) and (21).

V. MORI'S q -PHASE TRANSITIONS AND TSALLIS' q INDEX

About 15 years ago Mori and coworkers developed a broad thermodynamic formalism to characterize sharp changes at bifurcations and at other singular attractors in low dimensional maps [23]. The formalism was specially adapted to study critical attractors and was applied to the specific case of the onset of chaos in the circle map

at the golden mean [21], [23] and in the logistic map at the period doubling accumulation point [22], [23]. For critical attractors the scheme involves the evaluation of fluctuations of the generalized finite-time Lyapunov coefficient

$$\lambda_1(t; x_0) = \frac{1}{\ln t} \sum_{i=0}^{X-1} \ln \left| \frac{df(x_i)}{dx_i} \right| ; t \geq 1; \quad (22)$$

where $f(x)$ is a map with control parameter(s) tuned at a critical attractor. Notice the replacement of the customary t by $\ln t$ in Eq. (22), as the ordinary Lyapunov coefficient λ_1 vanishes for critical attractors at $t \rightarrow 1$.

The density distribution for the values of λ_1 at $t \rightarrow 1$, $P(\lambda_1; t)$, is written in the form [23], [21], [22]

$$P(\lambda_1; t) = t^{-\alpha} P(0; t); \quad (23)$$

where α is a concave spectrum of the fluctuations of λ_1 with minimum $\alpha(0) = 0$ and is obtained as the Legendre transform of the 'free energy' function $\phi(q)$, defined as $\phi(q) = \lim_{t \rightarrow 1} \frac{1}{\ln t} \ln Z(t; q) = \ln t$, where $Z(t; q)$ is the dynamic partition function

$$Z(t; q) = \int dP(\lambda_1; t) t^{q\lambda_1}; \quad (24)$$

The 'coarse-grained' function of generalized Lyapunov coefficients $\phi(q)$ is given by $\phi(q) = \int d\lambda_1 \phi(\lambda_1) \delta(q - \lambda_1)$ and the variance $v(q)$ of $P(\lambda_1; t)$ by $v(q) = \int d\lambda_1 \lambda_1^2 \phi(\lambda_1) \delta(q - \lambda_1)$ [23], [21], [22]. The functions $\phi(q)$ and α are the dynamic counterparts of the Renyi dimensions $D(q)$ and the spectrum $f(\lambda_1)$ that characterize the geometric structure of the attractor [2].

As with ordinary thermal 1st order phase transitions, a "q-phase" transition is indicated by a section of linear slope $m_c = 1 - q$ in the spectrum (free energy) $\phi(q)$, a discontinuity at $q = q_c$ in the Lyapunov function (order parameter) $\alpha(q)$, and a divergence at q_c in the variance (susceptibility) $v(q)$. For the onset of chaos at golden mean a single q-phase transition was numerically determined [23] and found to occur approximately at a value around $m_c = (1 - q_c)^{-1} \approx 0.95$. It was pointed out in Ref. [23] that this value would actually be $m_c = (1 - q_c)^{-1} = m_{ax} = 2^{-1} \approx 0.948997$. Our analysis below shows that this initial result gives a rough picture of the dynamics at the golden mean attractor and that actually an infinite family of q-phase transitions of decreasing magnitude takes place there.

From the results for $\alpha^{(k)}$ and $\lambda_1^{(k)}$ we can construct the two-step Lyapunov function

$$\lambda_1^{(2)}(t; x_0) = \begin{cases} < \frac{1}{q} & ; 1 < q < q_c \\ 0 & ; q_c < q < 2 - q_c \\ > \frac{1}{2 - q_c} & ; 2 - q_c < q < 1 \end{cases}; \quad (25)$$

where $\lambda_1^{(1)} = 2 \ln j_{gm} = \ln w_{gm} \approx 1.053744$ and $\lambda_1^{(2)} = w_{gm}^{-1} \lambda_1^{(1)} \approx 1.704994$. See Fig. 5a. Direct contact

can be established now with the formalism developed by Mori and coworkers and the q-phase transition reported in Ref. [21]. The step function for $\lambda_1^{(2)}$ can be integrated to obtain the spectrum $\phi^{(2)}(q) = \int d\lambda_1 \phi(\lambda_1) \delta(q - \lambda_1)$ and from this its Legendre transform $\alpha^{(2)}(\lambda_1) = \int d\phi(\phi) \delta(\lambda_1 - \phi)$. The free energy functions $\phi^{(2)}(q)$ and $\alpha^{(2)}(\lambda_1)$ obtained from the two-step $\lambda_1^{(2)}$ determined above are given by

$$\phi^{(2)}(q) = \begin{cases} < \frac{1}{q} & ; q < q_c \\ 0 & ; q_c < q < 2 - q_c \\ > \frac{1}{2 - q_c} & ; 2 - q_c < q < 1 \end{cases}; \quad (26)$$

and

$$\alpha^{(2)}(\lambda_1) = \begin{cases} (1 - q) & ; \lambda_1 < \frac{1}{q} < 0 \\ (1 - q) & ; 0 < \lambda_1 < \frac{1}{2 - q_c} \end{cases}; \quad (27)$$

See Fig. 5b. The constant slopes of $\alpha^{(2)}$ represent the q-phase transitions associated to trajectories linking two regions of the attractor, $\lambda_1' = 0$ (or $\lambda_1' = 1$) and $\lambda_1' = 1$, and their values $1 - q$ and $q - 1$ correspond to the index q obtained for the q-exponentials t^{λ_1} in Eqs. (17) and (20). The slope $q - 1 = m_{ax} = 2^{-1} \approx 0.949$ coincides with that originally detected in Ref. [21].

VI. DYNAMICS FROM THE TRAJECTORY SCALING FUNCTION

The trajectory scaling function $\chi(y)$ for the golden mean route is constructed [25], [26] via the evaluation of the ratios

$$\chi_n(m) = \frac{d_{n+1, m}}{d_{n, m}}; \quad (28)$$

where $d_{n, m} = j_m^{F_n + m}$, $j_m = 0; 1; 2; \dots$, and where the denominator is replaced by $d_{n, m} = j_m^{m F_n}$ in case $m = F_n$. The function $\chi(y)$ is obtained as the limit $\chi(y) = \lim_{n \rightarrow \infty} \chi_n(m)$ where $y = \lim_{n \rightarrow \infty} m = F_n$, and shows finite (jump) discontinuities at all rationals of the form $m = F_n$. The main discontinuity appears at $y = 0$, since $\chi(0) = j_{gm} j^1$ but $\chi(0^+) = j_{gm} j^3$, and again at $y = w_{gm}^2$. Other discontinuities in $\chi(y)$ appear at $y = w_{gm}, w_{gm}^3, w_{gm}^4, w_{gm} + w_{gm}^3, w_{gm} + w_{gm}^4$, etc., and of course $w_{gm} + w_{gm}^2 = 1$. We leave a detailed account of these properties to a later occasion [29]. In most cases it is only necessary to consider the first few as their magnitude decreases rapidly. See, e.g. Fig. 2 in Ref. [26]. The discontinuities of $\chi_n(m)$ can be suitably obtained by first generating the superstable orbit at λ_1 and then plotting the position differences $j_m - j$ for times of the form $t = F_n + m$, $n = 0; 1; 2; \dots$, in logarithmic scales. The distances that separate positions along the time subsequence correspond to the logarithm of the distances $d_{n, m}$. See Figs. 3 and 4 where the constant spacing of positions along the main diagonal provide the values for $\ln d_{n, 0} = n \ln j_{gm} j$ and $\ln d_{n, 1} = 3n \ln j_{gm} j$ respectively. The constant slope s_m of the resulting time subsequence data is related to $\chi_n(m)$, i.e. $\chi_n(m) = (w_{gm})^{s_m}$.

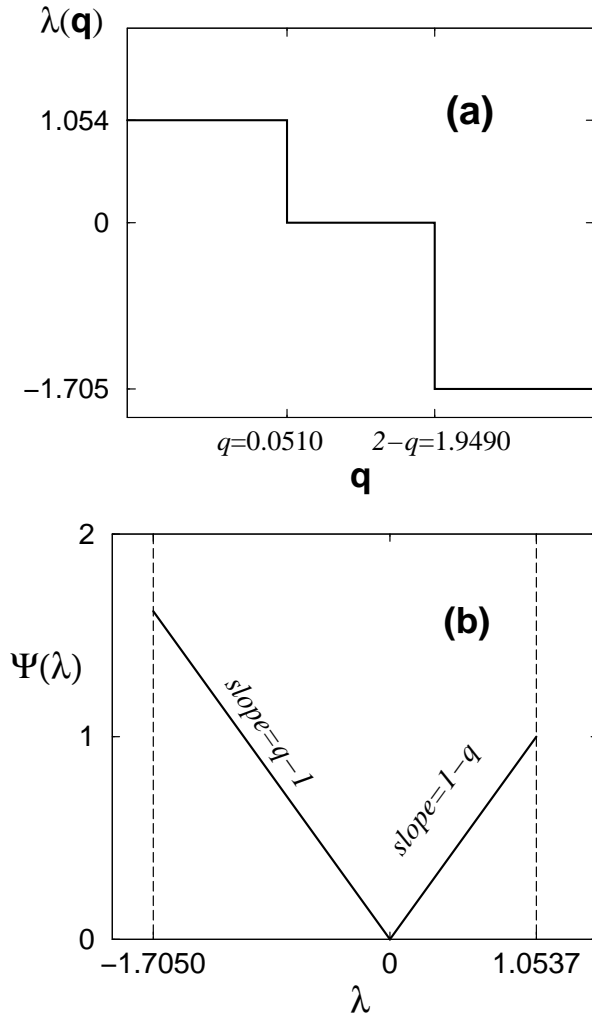


FIG. 5: q -phase transitions occurring at index values q and $2-q$. (a) The two-step Lyapunov function $\lambda(q)$. (b) The piece-wise spectrum $\Psi(\lambda)$. These transitions correspond to the main discontinuity in the trajectory scaling function $\tau_n(m)$. See text for details.

See Figs. 3 and 4 where the slopes of the main diagonal subsequences have the values $\ln j_{gm} = \ln w_{gm}$ and $3 \ln j_{gm} = \ln w_{gm}$, respectively. From these two slopes the value of the largest jump discontinuity of $\tau_n(m)$ is determined.

The sensitivity $\tau_n(0)$ can be evaluated for trajectories within the attractor via consideration of the discontinuities of $\tau_n(m)$. We expect the initial and the final separation of the trajectories to be the diameters $d_{n,m}(0) = d_{n,m}$ and $d_{n,m}(t) = d_{n,m+t}$, $t = F_n - 1$, respectively. Then, $\tau_n(0)$ is obtained as

$$\tau_n(0) = \lim_{n \rightarrow \infty} \frac{d_{n,m+t}^n}{d_{n,m}^n} : \quad (29)$$

Notice that in this limit $d_{n,m}(0) \rightarrow 0$, $t \rightarrow 1$ and the F_n -supercycle becomes the onset of chaos. Then, $\tau_n(0)$

can be written as

$$\tau_n(m) \sim \frac{(m-1)^n}{m^n} ; t = F_n - 1 \text{ and } n \text{ large}; \quad (30)$$

where we have used $j_n(m) \sim \prod_{i=1}^n d_{i+1,m} = d_{i,m}$ and $d_{i+1,m+F_n} = d_{i+1,m}$. Notice that for the inverse process, starting at $d_{n,m}(0) = d_{n,m+t} = d_{n,m-1}$ and ending at $d_{n,m}(t) = d_{n,m} = d_{n,m-1+t}$, with $t = F_n + 1$ one obtains

$$\tau_n(m-1) \sim \frac{(m-1)^n}{m^n} ; t = F_n + 1 \text{ and } n \text{ large}; \quad (31)$$

Therefore, from the properties of $\tau_n(m)$ we can determine those for τ_n . This function can be obtained at different levels of approximation by considering only a fixed number of its larger discontinuities. The discontinuities of $\tau_n(m)$ appear divided into two sets, the first falls on the interval $0 < y < w_{gm}^2$, and the second on $w_{gm}^2 < y < 1$. The amplitudes of the jumps in the second set are much smaller than those in the first set [26]. The simplest approximation for $\tau_n(m)$ is to consider only one jump in the first set at w_{gm}^2 and none in the second set, so that

$$\tau_n(m) = \begin{cases} 0^1 ; & 0 < y < w_{gm}^2 ; \\ 1^1 ; & w_{gm}^2 < y < 1 ; \end{cases} \quad (32)$$

where $0^1 = j_{gm}^3 \sim 2.139583$ and $1^1 = j_{gm} \sim 1.288575$. This level of approximation assumes that there are only two scaling factors, those associated to the most crowded and most sparse regions of the attractor. The next level of approximation for $\tau_n(m)$ involves two jumps in the first set at w_{gm}^3 and w_{gm}^2 , and still none in the second set, so that

$$\tau_n(m) = \begin{cases} 0^1 ; & 0 < y < w_{gm}^3 ; \\ 1^1 ; & w_{gm}^3 < y < w_{gm}^2 ; \\ 2^1 ; & w_{gm}^2 < y < w_{gm} ; \\ 3^1 ; & w_{gm} < y < 1 ; \end{cases} \quad (33)$$

where $0^1 = j_{gm}^3$, $1^1 = 1 = (w_{gm}^2)^1 \sim 2.452$, $2^1 = 1 = (w_{gm})^1 \sim 1.430$ and $3^1 = j_{gm} \sim 1.288575$. The two additional scaling factors correspond to two 'midway' regions of the attractor. More accurate approximations to $\tau_n(m)$ can be constructed by incorporation of additional discontinuities. Note that the number of discontinuities increase in each set as $F_M - 1, M = 1, 2, \dots$.

Use of Eq. (32) in Eqs. (30) and (31) (together with Eq. (16)) recovers our previous results for τ_n and q in Eqs. (17) to (21), and therefore also those for $\lambda(q)$, $\Psi(\lambda)$ in Eqs. (25) to (27). When use is made of Eq. (33) in Eqs. (30) and (31) we obtain three values for the q index, q_1, q_2 and q_3 (together with the conjugate values $2-q_1, 2-q_2$ and $2-q_3$ for the inverse trajectories). For each value of q there is a set of q -Lyapunov coefficients running from a maximum $q_{j,m}^{ax}$ to zero (or a minimum $q_{j,m}^{in}$ to zero). From the results for $q_j^{(k)}$ and $2-q_j^{(k)}$,

$j = 0; 1; 2$, we can construct three Lyapunov functions $\lambda_j(q)$, $1 < q < 1$, each with two jumps located at $q = q_j = 1 - \ln 2 = \ln q_{j+1}$ and $q = 2 - q_j$. We obtain a couple of two q -phase transitions for each of the three values of the q index, q_0 , q_1 and q_2 . The constant slope values for the q -phase transitions at $1 - q_j$ and $q_j - 1$ appear again, but now we have two other pairs of transitions with slope values $1 - q_j$ and $q_j - 1$, and, $1 - q_j$ and $q_j - 1$, that correspond, respectively, to orbits that link the most crowded region of the attractor to the 'medium crowded' region, and to orbits that link the 'medium sparse' region with the 'most sparse' region of the attractor. Similar but more elaborated results are obtained when more discontinuities in $\lambda_j(y)$ are taken into account. These results reflect the multi-region nature of the multifractal attractor and the memory retention of these regions in the dynamics. Thus, when $\lambda_j(y) = \lambda_j(y')$ one has $\tau = 1$ (or $\lambda_j(0) = 0$) which corresponds to trajectories that depart and arrive in the same region, when $\lambda_j(y) \neq \lambda_j(y')$ the power laws in Eqs. (30) and (31) correspond to a departing position in one region and arrival at a different region and vice versa, the trajectories expand in one sense and contract in the other.

V II. S U M M A R Y

We have looked in some detail at the structure of the superstable orbit at the golden mean critical attractor for zero-slope cubic inflection point maps. This structure helped us determine the sensitivity to initial conditions for sets of starting positions within the attractor. We found that τ is made up of a hierarchy of families of infinitely many interconnected q -exponentials. Each pair of regions in the multifractal attractor, that contain the starting and finishing positions of a set of trajectories, leads to a family of q -exponentials with a fixed value of the index q and an associated spectrum of q -Lyapunov coefficients $\lambda_q^{(k)}$. The indexes q and the spectra $\lambda_q^{(k)}$ come in pairs, q and $2 - q$, and $\lambda_q^{(k)}$ and $\lambda_{2-q}^{(k)}$, as these correspond to switching starting and finishing trajectory positions. This dynamical organization is difficult to resolve from the consideration of a straightforward time evolution, i.e. the record of positions at every time t for a trajectory started at an arbitrary position (0) within the attractor. In this case what is observed [21] are strongly

fluctuating quantities that persist in time with a scrambled pattern structure that exhibits memory retention. Unsystematic averages over (0) would rub out the details of the multiscale dynamical properties we uncovered. On the other hand, if specific initial positions with known location within the multifractal are chosen, and subsequent positions are observed only at pre-selected times, when the trajectories visit another selected region, a distinct q -exponential expression for τ is obtained.

Subsequently, we explained that the above described properties for the sensitivity show up as sets of dynamical phase transitions. The dynamics consists of an infinite family of Mori's q -phase transitions, each associated, as before, to trajectories that have common starting and finishing positions located at specific regions of the attractor. The specific values of the variable q in the formalism of Mori and colleagues at which the q -phase transitions take place are the same values for the Tsallis entropic index q in τ . The transitions come in pairs at q and $2 - q$ as they are tied down to the expressions for $\lambda_q^{(k)}$ in τ . The dominant dynamical transition is associated to the most crowded and sparse regions of the attractor and the values of its relevant parameters coincide with those found in an earlier study with the use of Mori's coarse-grained formalism [21]. Here we have determined the q -phase transitions via the direct evaluation of the spectra $\lambda_q^{(k)}$ and $\lambda_{2-q}^{(k)}$ in τ .

Our results clearly apply to many other families of maps with zero slope inflection points of cubic nonlinearity and are likely to hold also for general nonlinearity $z > 1$. These results may be of relevance in condensed matter problems where the quasiperiodic route to chaos is involved. One interesting example is the phenomenon of the localization transition for transport in incommensurate systems, where Schrodinger equations with quasiperiodic potentials [30] are equivalent to nonlinear maps with a quasiperiodic route to chaos, and where the divergence of the localization length translates into the vanishing of the ordinary Lyapunov coefficient [31]. Our findings are very similar to those recently determined for the Feigenbaum attractor in unimodal maps [15], and reinforce the notion of generality of our identification of the source for the entropic index q observed at critical attractors.

Acknowledgments. Partially supported by CONACYT and DGAPA-UNAM, Mexican agencies.

-
- [1] H.G. Schuster, Deterministic Chaos. An Introduction, 2nd Revised Edition (VCH Publishers, Weinheim, 1988).
 [2] C. Beck and F. Schlogl, Thermodynamics of Chaotic Systems (Cambridge University Press, UK, 1993).
 [3] R.C. Hilborn, Chaos and nonlinear dynamics, 2nd Revised Edition (Oxford University Press, New York, 2000).
 [4] C. Tsallis, A.R. Plastino and W.-M. Zheng, Chaos, Solitons and Fractals 8, 885 (1997).
 [5] M.L. Lyra and C. Tsallis, Phys. Rev. Lett. 80, 53 (1998).
 [6] U. Timakli, C. Tsallis and M.L. Lyra, Eur. Phys. J. B 11, 309 (1999).
 [7] F.A.B.F. de Moura, U. Timakli and M.L. Lyra, Phys. Rev. E 62, 6361 (2000).
 [8] F. Baldovin and A. Roldo, Phys. Rev. E 66, 045104 (R) (2002).
 [9] F. Baldovin and A. Roldo, Phys. Rev. E 69, 045202 (R) (2004).
 [10] E.M. Ayoral and A. Roldo, Physica A 340, 219 (2004).

- [11] A. Robledo, *Physica D* 193, 153 (2004).
- [12] F. Baldovin and A. Robledo, *Europhys. Lett.* 60, 518 (2002).
- [13] A. Robledo, *Molec. Phys.* (in press) and [cond-mat/0504044](https://arxiv.org/abs/cond-mat/0504044).
- [14] A. Robledo, *Phys. Lett. A* 328, 467 (2004); F. Baldovin and A. Robledo, [cond-mat/0504033](https://arxiv.org/abs/cond-mat/0504033).
- [15] E. M. Ayoral and A. Robledo, *Phys. Rev. E* (in press) and [cond-mat/0501366](https://arxiv.org/abs/cond-mat/0501366).
- [16] C. Tsalis, *J. Stat. Phys.* 52, 479 (1988).
- [17] For recent reviews see, *Nonextensive Entropy { Interdisciplinary Applications*, M. Gell-Mann and C. Tsalis, eds., (Oxford University Press, New York, 2004). See <http://tsallis.cat.cbpf.br/biblio.htm> for full bibliography.
- [18] C. Grebogi, E. Ott, S. Pelikan, and J.A. Yorke, *Physica D* 13, 261 (1984).
- [19] P. Grassberger and M. Scheunert, *J. Stat. Phys.* 26, 697 (1981).
- [20] G. Anania and A. Politi, *Europhys. Lett.* 7, 119 (1988). This work headed the determination of the spectrum of anomalous Lyapunov coefficients at the onset of chaos in the logistic map.
- [21] T. Horita, H. Hata, H. Mori and K. Tomita, *Prog. Theor. Phys.* 81, 1073 (1989).
- [22] H. Hata, T. Horita and H. Mori, *Prog. Theor. Phys.* 82, 897 (1989).
- [23] H. Mori, H. Hata, T. Horita and T. Kobayashi, *Prog. Theor. Phys. Suppl.* 99, 1 (1989).
- [24] M. J. Feigenbaum, *Commun. Math. Phys.* 77, 65 (1980); *Physica D* 7, 16 (1983).
- [25] M. J. Feigenbaum, in *Proceedings of the 1984 Latin American School of Physics*, Santiago, Chile, F. Claro, Editor (Springer-Verlag, Berlin, 1985).
- [26] R. Mainieri, *Phys. Rev. E* 48, 898 (1993); R. Mainieri and R. E. Ecke, *Physica D* 79, 193 (1994).
- [27] M. H. Jensen, L. P. Kadanoff, A. Libchaber, I. Procaccia and J. Stavans, *Phys. Rev. Lett.* 55, 2798 (1985).
- [28] M. J. Feigenbaum, L. P. Kadanoff and S. J. Shenker, *Physica D* 5, 370 (1982).
- [29] H. Hernandez-Saldana and A. Robledo, in preparation.
- [30] P. G. Harper, *Proc. Phys. Soc., London, Sect. A* 68, 874 (1955).
- [31] J.A. Katořa and I.I. Satić, *Physica D* 109, 70 (1997).